J. Astrophys. Astr. (2020) 41:50
https://doi.org/10.1007/s12036-020-09672-5

© Indian Academy of Sciences

Oxygen abundances of carbon-enhanced stellar population in the halo

A. SUSMITHA[1,*], T. SIVARANI[2], D. K. OJHA[1], JOE P. NINAN[3,4], A. BANDYOPADHYAY[2], A. SURYA[5] and U. ATHIRA[2]

[1]Department of Astronomy and Astrophysics, Tata Institute of Fundamental Research, Colaba, Mumbai 400005, India.
[2]Indian Institute of Astrophysics, Sarjapur Road, Koramangala, Bengaluru 560034, India.
[3]Department Of Astronomy and Astrophysics, The Pennsylvania State University, 525 Davey Laboratory, University Park, PA 16802, USA.
[4]Center for Exoplanets and Habitable Worlds, The Pennsylvania State University, 525 Davey Laboratory, University Park, PA 16802, USA.
[5]Center for Astrophysics and Space Sciences, University of California, San Diego, CA 92093, USA.
Corresponding author. E-mail: susmitha.antony@tifr.res.in

MS received 5 September 2020; accepted 5 October 2020; published online 18 December 2020

Abstract. The large fraction of carbon-enhanced metal-poor (CEMP) stars at lower metallicities makes them an interesting class of objects to be probed further in greater detail. They show different abundance patterns of neutron-capture elements and based on that CEMP stars are further divided into four categories. Abundances of C, N and O, along with other elements, are required to understand the different nucleosynthetic origins of the subclasses and their progenitors. We studied nine bright carbon-enhanced stars from the Milky Way halo in a metallicity range from −0.8 to −2.5. They show enhancement in C, N, O and Ba and exhibit radial velocity variation. This indicates the presence of a binary companion which might have contributed to the enhanced carbon and s-process abundance through mass transfer during its asymptotic-giant-branch (AGB) phase of evolution. Their abundance pattern of C, N and O favors low-mass nature for their binary companion.

Keywords. Abundances—AGB stars—s-process—carbon-enhanced—oxygen abundance.

1. Introduction

Various large-scale spectroscopic surveys such as Hamburg/ESO survey (HES, Christlieb *et al.* 2001), HK survey (Beers *et al.* 1992) and SDSS-SEGUE survey (Yanny *et al.* 2009) probed the metal-poor population of stars in the Milky Way halo and identified that a considerable fraction of the metal-poor population shows enhancement in surface carbon abundance. The fraction of carbon-enhanced population has been found to be 20% for stars with metallicity < -2.0 (Lucatello *et al.* 2005, 2006; Aoki *et al.* 2013; Yong *et al.* 2013), and the fraction increases with decreasing metallicity (Placco *et al.* 2014). This subset of metal-poor stars with [C/Fe] > 0.7 and [Fe/H] < -2.0 is classified as carbon-enhanced metal-poor (CEMP) stars (Aoki *et al.* 2007) and are of great interest to the astronomy community due to their high carbon abundance and the sizable fraction in the low-metallicity regime. Several follow-up high-resolution studies showed that CEMP stars may have four different abundance patterns of the heavy elements and were grouped as: CEMP-s stars, which show an enhancement of heavy elements produced by slow-neutron-capture process (e.g. Ba); CEMP-r stars, with enhancement of elements formed by rapid-neutron-capture process (e.g. Eu); CEMP-rs stars, which exhibit an excess abundance of both slow and rapid neutron-capture processes; and CEMP-no stars, which do not

This article is part of the Topical Collection: Chemical elements in the Universe: Origin and evolution.

show any enhancement of neutron-capture elements. Around 80% of the CEMP population is constituted by CEMP-s subclass (Aoki *et al.* 2007), and multi-epoch observations of these samples demonstrated that the majority of stars in the CEMP-s class are members of binary systems (Lucatello *et al.* 2005; Starkenburg *et al.* 2014). This favors the idea of AGB binary mass transfer, and the more massive companion star would be expected to have evolved to a cool white dwarf (Bisterzo *et al.* 2012; Abate *et al.* 2015 and references therein). While the origin of carbon in CEMP-r stars remains unknown, CEMP-rs stars were identified to be showing radial velocity variations indicating that carbon and s-process abundance would have similar origin as in CEMP-s stars (Sivarani *et al.* 2004; Masseron *et al.* 2010; Bisterzo *et al.* 2011). However, the enhancement in r-process elements (e.g. Eu) is still a matter of debate. On the other hand, CEMP-no stars are often found not to be associated with binaries (Hansen *et al.* 2016b, with a few exceptions for the non-binarity including the CEMP-no stars studied in Dearborn *et al.* (1986), Starkenburg *et al.* (2014), Hansen *et al.* (2016b), Caffau *et al.* (2016)) and Bandyopadhyay *et al.* (2018)) thus they reflect the ISM abundance from which the stars were born. Models of faint supernovae that experienced mixing and fall-back and models of zero-metallicity-spin stars having high rotational velocity could explain the peculiar abundance patterns shown by CEMP-no stars (Umeda and Nomoto 2003; Meynet *et al.* 2006; Hansen *et al.* 2016a; Yoon *et al.* 2016; Susmitha *et al.* 2017).

Even though the viable astrophysical processes as a source of carbon in CEMP stars are identified, the masses of progenitors and multiple nucleosynthesis processes/sites to explain the varied abundance pattern in the light and heavy elements are still unknown.

To understand the nature of progenitor, we require abundances of C, N and O of a large sample of CEMP stars, along with other elemental abundances. Carbon and nitrogen abundance can be determined from medium-resolution optical spectra of CEMP stars using the CH, C_2 and CN features (among cooler CEMP stars). Oxygen abundance is usually determined using the forbidden lines at 6300 Å or 6363 Å or oxygen triplet at 7770 Å region. The triplet around 7770 Å suffers non-local thermodynamic equilibrium (NLTE) effects so the only reliable measurements are from the forbidden oxygen lines. These lines are weaker in giants and at lower metallicities. Clear detection of [O I] lines requires several hours of integration even with 8–10 m class telescopes. Also, these lines are located in a region where there are a plethora of CN molecular features. So, not many dedicated oxygen measurements were performed for CEMP stars, except by Kennedy (2011), who performed oxygen abundance estimates using near-infrared (NIR) CO molecular features for 57 CEMP stars. But it is still uncertain that the oxygen abundances derived from optical [O I] lines and NIR CO molecular feature are consistent or not. In this paper, we discuss the oxygen abundance of a few carbon-enhanced population at different metallicities to constrain the characteristics of their progenitor along with the abundance of other elements, including C, N and Ba.

2. Observation and data reduction

Since the primary aim of this study is to understand the consistency of measurements of oxygen abundance using different techniques, we preselected those samples from the literature whose oxygen abundance was not reported earlier or have already been derived using spectral features other than the [O I] lines. We included only brighter candidates (Vmag $<$ 13) with different metallicities to ensure that [O I] lines would have enough strength to be used for accurate abundance analysis.

The observations of these objects were taken using Hanle Echelle Spectrograph (HESP) mounted on 2 m Himalayan Chandra Telescope (HCT) at Hanle. The spectrograph has two resolution modes and we used the low-resolution mode (R=30000) for our observations to cover objects with good signal-to-noise ratio. The objects were observed in multiple frames of 40-minute exposure depending on the brightness. The objects were observed in the star-sky mode of the spectrograph, which enabled the sky to be subtracted from the object fiber. ThAr spectrum was taken at the end of each object spectrum for the wavelength calibration. The spectral reduction included trimming, bias subtraction, aperture extraction and wavelength calibration. We used PyRAF[1] to perform these steps. The final normalized and co-added spectrum covers the wavelength range 3800–10500 Å.

3. Stellar parameters and chemical abundances

The spectra of carbon-enhanced stars are dominated by different carbon molecular features. This hampers getting clean lines for deriving abundances using the

[1]PyRAF is a product of the Space Telescope Science Institute, which is operated by AURA for NASA.

equivalent-width method. Hence, throughout the analyses, we used the spectral-synthesis method to derive the abundances of key elements. We used the TURBOSPECTRUM code developed by Plez (2012) to derive stellar parameters and abundances. The stellar atmospheric models from Mészáros *et al.* (2012) were used in which ATLAS9 and MARCS codes are modified with a wide range of carbon and α-element enhancements and with an updated H_2O line list. We assumed local thermodynamic equilibrium (LTE) for all species, and solar abundances were adopted from Asplund *et al.* (2009). We have also accounted for hyperfine structure for Ba even though the corrections are negligible. We used the CH molecular line list compiled by T. Masseron (priv. comm.) and CN molecular data from Plez & Cohen (2005). For the case of C_2 molecular features, the line list was taken from Kurucz database[2].

3.1 *Stellar parameters*

We used J-H, J-K and V-K colors to derive the effective temperature of the program stars using the color transformation relations given in (Alonso *et al.* 1996, 1999). We adopted the temperature derived from V-K color as the final effective temperature (T_{eff}) of the samples due to its larger wavelength span. The other color temperatures differ by 150 K from the final T_{eff} and this is quoted as the uncertainty in the temperature measurements. The final T_{eff} values of the samples range from 3700 K to 4645 K.

Mg II triplet around 5172 Å is used to derive the surface gravity, log *g*. For this, we used a synthetic grid of model spectra for various values of log *g* with a step size of 0.25 dex. The best-fit model value was chosen as the final log *g* (refer Figure 1). We also fitted the C_2 molecular bandhead at 5165 Å while deriving the log *g* to converge onto the best-fit parameters. The final derived values range from 0.2 to 3.5, indicative of their red-giant-branch (RGB) phase of evolution. We derived the metallicity by fitting cleaner Fe features in the spectra to which the contribution of molecular feature is low or negligible. For this, we synthesized the whole region of the spectrum without inputting the atomic line list and identified the clean Fe lines where the molecular contributions to the continuum are negligible. We fixed the microturbulent velocity by iteratively fitting the less strong and clean Fe I features and the best-fit value was adopted as the final value. The details of the stellar parameters are given in Susmitha *et al.* (2020) (submitted).

[2] http://kurucz.harvard.edu/linelists/linesmol/

3.2 *Abundances of C, N, O and Ba*

We fitted the C_2 molecular band heads at 5165 Å and 5635 Å to derive the C abundance and retrieved the same abundance values and quoted them as the final abundance of C for the respective samples. The uncertainty of C abundance measurement is 0.2 dex as this difference brings a noticeable change in the molecular features (see Figure 2).

To derive the N abundance, we fitted CN molecular features spanning from 5635 Å to 6700 Å by repeatedly varying the N abundance with a step size of 0.2 dex and kept a fixed C abundance that is derived from the C_2 molecular band (Figure 2). We derived the oxygen abundance of the sample stars by fitting the [O I] features at 6300 Å or/and 6363 Å (refer Figure 3) .

Since these lines are blended with CN features, any small change in N abundance results in inaccurate measurements of the O abundance. So we fixed the C abundance and iteratively changed the N and O abundances without affecting the other CN features in the spectra. The resulting abundance measurements from both the O features differ by 0.3 dex due to the recursion process. We take this difference as the uncertainty in the N and O abundances.

We measured the abundance of Ba using various Ba II lines such as 5853 Å, 6142 Å and 6497 Å. All the samples in the study were identified to be showing an enhancement in Ba abundance. Since Ba is a representative element for s-process nucleosynthesis, it is an indication of occurrence of the slow-neutron-capture process in the progenitor. We have also measured abundances of other neutron-capture elements, and the details of those are given in Susmitha *et al.* (2020) (submitted).

We have also estimated the radial velocity of all the nine objects in this study and found that the radial velocity shows variation compared with the literature values.

4. Discussion and conclusion

We derived C, N, O and Ba abundances of nine carbon-enhanced stars having different metallicities ranging from −0.8 to −2.5. All the objects in this study show enhancement in these elements with

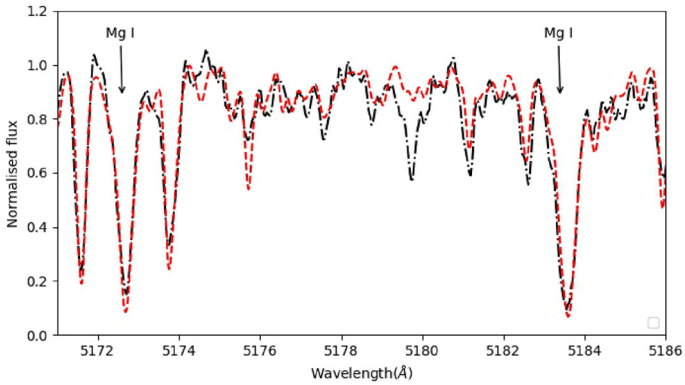

Figure 1. The Mg I lines at 5172 Å and 5183 Å in the spectrum of HE 1152-0355 fitted with the synthetic spectrum generated using the final adopted stellar parameters; T_{eff} = 4200 K, log g = 0.25, [Fe/H] = − 1.7, and microturbulent velocity ξ = 2.2 km/s.

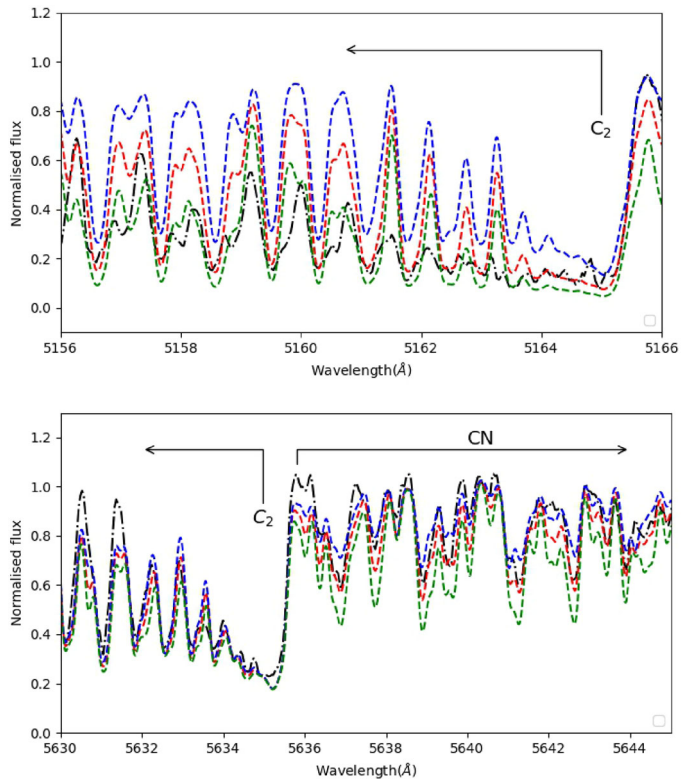

Figure 2. The C_2 and CN molecular features in the spectrum of HE 1152-0355 fitted with the synthetic spectrum generated using the final adopted C and N abundances. The red spectrum corresponds to the best-fit values [C/Fe] = 1.3 and [N/Fe] = 0.9. In the top panel, the blue and green spectra correspond to ± 0.2 dex, which is the expected uncertainty in carbon; this is calculated keeping the N abundance constant. In the bottom panel, the C abundance is kept constant and uncertainty of ± 0.3 dex is employed for the N abundance.

respect to Fe. The carbon enhancement together with enhancement in s-process elements and radial-velocity variations favor the scenario that the carbon-enhanced star is in a binary system. The companion star, during the AGB evolutionary phase, synthesised carbon and s-process elements in the intershell region and the same were brought to the surface during third-dredge-up (TDU) episodes. The mass transfer of these carbon and s-process-rich material from the AGB companion has contributed to the peculiar (C and s-process-rich) abundance among the carbon-enhanced stars studied here.

The C, N and O abundance pattern of our samples compared with the pattern produced by models of

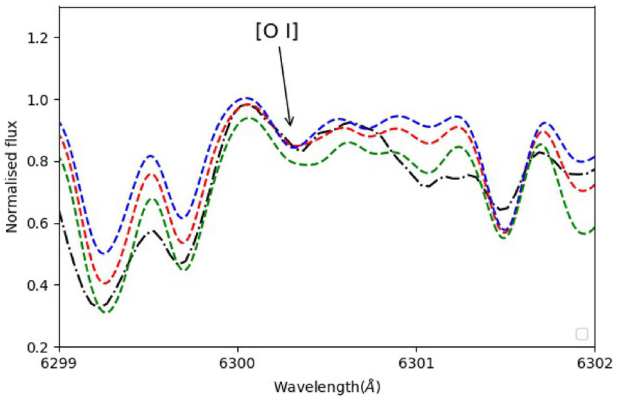

Figure 3. The [O I] line at 6300.3 Å in the spectrum of HE 1152-0355 (in black) fitted with synthetic spectra having different O abundances. The best-fit value of [O/Fe] = 0.5 is plotted in red. The green and blue spectra indicate syntheses corresponding to the range of uncertainty of ± 0.3 dex in oxygen abundance. The poor fitting of CN molecular features around [O I] comes from the change in the oxygen abundance.

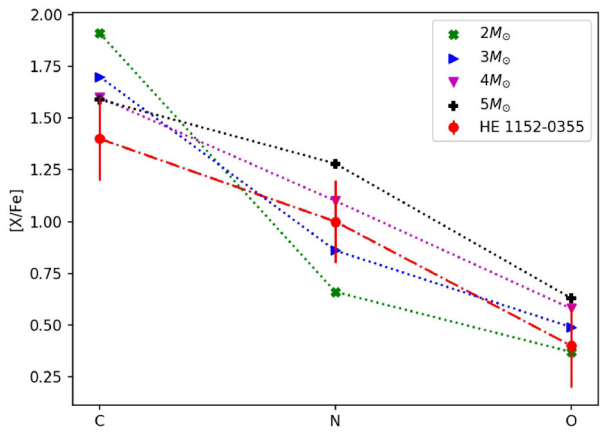

Figure 4. The C, N and O abundances of one of the carbon-enhanced stars, HE 1152-0355, compared with the AGB model values of different masses. We used the models from FRUITY database (Cristallo *et al.* 2011, 2015). Different colors and symbols are given for different masses. The red filled circles represent the values corresponding to the observed star. The abundance pattern matches with the models of low-mass AGB stars.

AGB stars shows more resemblance with that of low-mass AGB stars than a massive AGB star (refer Figure 4).

None of the objects show [C/N] <-0.5 and [hs/ls] >0.5 (hs denotes heavy s-process elements whereas ls denotes light s-process elements) simultaneously. This provides an extra confidence that the hot bottom burning (HBB) did not occur in the binary companion of our samples that would have resulted in an enormous amount of N compared to C and is a characteristic feature of a more massive ($M \geq 4M_{\odot}$) AGB star. So the mass range of the binary companion can be constrained to be $\leq 4M_{\odot}$. Various mechanisms such as cool-bottom-processing and proton-ingestion episodes can be suggested to explain the observed abundance pattern in these CEMP stars. The details are explained in Susmitha *et al.* (2020) (submitted).

Acknowledgements

We thank the staff of IAO, Hanle, and CREST, Hosakote, who made these observations possible. The facilities at IAO and CREST are operated by the Indian Institute of Astrophysics, Bengaluru. A.S. and D.K.O. acknowledge the support of the Department of Atomic Energy, Government of India, under Project No. 12-R&D-TFR-5.02-0200.

References

Abate C., Pols O. R., Karakas A. I., Izzard R. G. 2015, A&A, 576, A118
Alonso A., Arribas S., Martinez-Roger C. 1996, A&A, 313, 873
Alonso A., Arribas S., Martinez-Roger C., 1999, A&AS, 139, 33
Aoki, W., Beers, T. C., Christlieb, N., *et al.* 2007, ApJ, 655, 492
Aoki, W., Beers, T. C., Lee, Y. S., *et al.* 2013, AJ, 145, 13
Asplund, M., Grevesse, N., Sauval, A. J., & Scott, P. 2009, ARA&A, 47, 481
Bandyopadhyay, A., Sivarani, T., Susmitha, A., *et al.* 2018, ApJ, 859, 114
Bisterzo, S., Gallino, R., Straniero, O., Cristallo, S., & Käppeler, F. 2011. MNRAS, 418, 284
Bisterzo S., Gallino R., Straniero O., Cristallo S., Kappeler F., 2012, MNRAS, 422, 849
Beers, T. C., Preston, G. W., & Shectman, S. A. 1992, AJ, 103, 1987
Caffau, E., Bonifacio, P., Spite, M., *et al.* 2016, A&A, 595, L6
Christlieb, N., Green, P. J., Wisotzki, L., & Reimers, D. 2001, A&A, 375, 366
Cristallo, S., Piersanti, L., Straniero, O., *et al.* 2011, ApJS, 197, 17
Cristallo, S., Straniero, O., Piersanti, L., & Gobrecht, D. 2015, ApJS, 219, 40
Dearborn, D. S. P., Liebert, J., Aaronson, M., *et al.* 1986, ApJ, 300, 314
Hansen, C. J., Nordström, B., Hansen, T. T., *et al.* 2016a, A&A, 588, A37

Hansen, T. T., Andersen, J., Nordström, B., *et al.* 2016b, A&A, 586, A160
Kennedy C. R., *et al.*, 2011, AJ, 141, 10
Lucatello, S., Tsangarides, S., Beers, T. C., *et al.* 2005, ApJ, 625, 825
Lucatello, S., Beers, T. C., Christlieb, N., *et al.* 2006, ApJ, 652, L37
Masseron, T., Johnson, J. A., Plez, B., *et al.* 2010, A&A, 509, A93
Mészáros, S., Allende Prieto, C., Edvardsson, B., *et al.* 2012, AJ, 144, 120
Meynet, G., Ekström, S., & Maeder, A. 2006, A&A, 447, 623
Placco, V. M., Frebel, A., Beers, T. C., & Stancliffe, R. J. 2014, ApJ, 797, 21
Plez, B. 2012, Astrophysics Source Code Library [record ascl:1205.004]
Plez, B., & Cohen, J. G. 2005, A&A, 434, 1117
Sivarani, T., Bonifacio, P., Molaro, P., *et al.* 2004, A&A, 413, 1073
Starkenburg, E., Shetrone, M. D., McConnachie, A. W., & Venn, K. A. 2014, MNRAS, 441, 1217
Susmitha, A., Koch, A., & Sivarani, T. 2017, A&A, 606, A112
Susmitha, A., Ojha, D.K., Sivarani, T., Nainan, J.P., Bandyopadhyay, A., Surya, A., Unni, A. 2020, MNRAS (Submitted)
Umeda, H., & Nomoto, K. 2003, Nature, 422, 871
Yanny, B., Rockosi, C., Newberg, H. J., *et al.* 2009, AJ, 137, 4377
Yong, D., Norris, J. E., Bessell, M. S.,*et al.* 2013, ApJ, 762, 26
Yoon, J., Beers, T. C., Placco, V. M.,*et al.* 2016, ApJ, 833, 20 Meszaros